Automatic Computation of the Posterior Nipple Line from Mammographies

Quynh Nhu Jennifer Tran[1], Tina Santner[2][a] and Antonio Rodríguez-Sánchez[1][b]

[1]*Department of Computer Science, University of Innsbruck, Innsbruck, Austria*
[2]*Department of Radiology, Medical University of Innsbruck, Innsbruck, Austria*

Keywords: Mammogram, Posterior Nipple Line Detection, Computer Vision.

Abstract: Breast cancer is the most commonly diagnosed cancer in female patients. Detecting early signs of malignity by undergoing breast screening is therefore of great importance. For a reliable diagnosis, high-quality examinated mammograms are essential since poor breast positioning can cause cancers to be missed, which is why mammograms are subject to strict evaluation criteria. One such criterion is the posterior (or pectoralis) nipple line (PNL). We present a method for computing the PNL length, which consisted of the following steps: Pectoral Muscle Detection, Nipple Detection, and final PNL Computation. A multidirectional Gabor filter allowed us to detect the pectoral muscle. For detecting the nipple we made use of the geometric properties of the breast, applied watershed segmentation and Hough Circle Transform. Using both landmarks (pectoral muscle and nipple), the PNL length could be computed. We evaluated 100 mammogram images provided by the Medical University of Innsbruck. The computed PNL length was compared with the real PNL length, which was measured by an expert. Our methodology achieved an absolute mean error of just 6.39 mm.

1 INTRODUCTION AND BACKGROUND

Breast cancer is the most commonly diagnosed cancer in women, accounting for 11.7% of all cancer cases in 2020 with approximately 2.3 million new cases worldwide. According to GLOBOCAN 2020, a database on cancer statistics, breast cancer is also the fifth leading cause of cancer mortality with about 685,000 new deaths (Sung et al., 2021).

Early signs of malignity can be detected by examining screening mammograms, which are X-ray images of the breast. The ability to make reliable diagnoses strongly depends on the quality of the mammograms, where correct breast positioning is particularly important, as poor positioning of the breast can contribute to breast cancers being missed. Several tools are available to check and monitor this diagnostic image quality. These are checklists or classification systems, where several image quality statements are assessed and the images are classified based on the overall score (Waade et al., 2021). Well-known and internationally (NHSBSP, 1989) in use is the PGMI

(perfect-good-moderate-inadequate) (Klabunde et al., 2001). One positioning criterion of this system is the posterior (or pectoralis) nipple line (PNL). The PNL is a line drawn posteriorly and perpendicularly from the nipple towards the pectoral muscle. Ideally, the PNL in the craniocaudal (CC) view should be the same length as the PNL in the mediolateral oblique (MLO) view to ensure that sufficient breast tissue is included, and a reliable diagnosis can be made (Sweeney et al., 2017). However, the problem is that measuring the PNL for both views manually is time-consuming. In addition, the results are subjective and inhomogeneous and can vary from person to person.

Recent approaches have been proposed for automated assessment of the breast positioning quality in mammograms based on deep learning. (Gupta et al., 2020) used transfer learning to predict the two points representing the PNL in the MLO view. He used Inception-V3 (Szegedy et al., 2015) as the base network and replaced the last layer with a single output node. The network was initialized with the pretrained weights from the ImageNet dataset (Deng et al., 2009). For detecting the PNL in the CC view, an algorithm was developed for detecting the radiopaque marker, which was placed over the nipple during the

[a] https://orcid.org/0000-0002-2224-1089
[b] https://orcid.org/0000-0002-3264-5060

data labeling step, using Hough Circle Transform. The final PNL was a line drawn horizontally from the radiopaque marker to the image border. Brahim et al. (2022) trained a convolutional neural network for binary classification. The output was either 0 (good breast positioning) or 1 (poor breast positioning). Hejduk et al. (2023) trained eight deep convolutional neural networks for detecting the presence of anatomical landmarks and localizing features. Three of the features are the nipple, pectoralis cranial, and the pectoralis caudal. Based on them the PNL length could be calculated.

Even though providing very good results, deep learning is limited when the quantity of images is limited or the intermediate steps - i.e. image landmarks - are not provided, but just the final PNL values.

In this paper, we present a method to automatically compute the length of the PNL in mammograms without the need for a large labelled dataset containing image landmarks. The proposed method can help in assessing the image quality of mammograms by automatically measuring the PNL length and thus saving time. This is done by first detecting the pectoralis major (pectoral) muscle and the location of the nipple using computer vision-based methods, which once successfully detected, the PNL length can be accurately calculated. All images used in this paper are from the dataset provided by the Medical University of Innsbruck.

2 METHODS

Our method for Pectoral Muscle Detection follows a similar approach to the multidirectional Gabor filter (MDGF)-based approach for pectoral muscle boundary (PMB) detection by (Rahman and Jha, 2022) and is explained next.

2.1 Region of Interest (ROI) Extraction

In the MLO view, the pectoral muscle usually lies in the upper left corner, and therefore a triangular ROI containing the PMB was computed. For this, the image was converted into a binary image by applying simple thresholding with a threshold value of 2. Afterwards, the border following algorithm (Suzuki and Keiichi, 1985) was applied on the binary image to retrieve contours, and the contour with the largest area was selected to be the one of the breast boundary. Next, a mask was created by filling the area bounded by the contour. The Harris Corner Detector algorithm (Harris and Stephens, 1988) was then applied to the mask, where only significant corners

were selected. Only pixels where the Harris corner response was greater than 20% of the maximum response value were considered. The corner with the smallest Euclidean distance to the top-right corner of the image was then selected. Finally, the triangular ROI was defined by the three corner points: top-left corner, bottom-left corner, and the computed corner marking the starting point of the breast boundary.

2.1.1 ROI Preprocessing

To increase the image contrast, Contrast Limited Adaptive Histogram Equalization (CLAHE) (Pizer et al., 1987) was applied to the ROI with a contrast limiting threshold of 1 and 8×8 tile size. To further enhance the ROI, Non-Local Means Denoising (Buades et al., 2011) was used to reduce noise. The filter strength was set to 10 since a higher value would remove important details. Besides low contrast and noise, breast tissue can pose a challenge in cases where it overlaps with the PMB. To address this problem, we applied image inpainting which can restore selected regions in an image by filling them with the information surrounding them (Bertalmio et al., 2000). Since breast tissue usually has higher pixel intensities than the muscle region, top-hat filtering (computes the opening of an image by removing small objects from the foreground, and subtracts it from the original image) was applied to the denoised ROI to enhance small bright objects. Then simple thresholding was performed on the transformed ROI with a threshold value of 9. The resulting thresholded image indicates which regions needed to be restored and was passed as an inpainting mask to the inpainting function.

The ROI image might contain regions of 0-pixels like the background in mammograms. A strong intensity edge between the 0-pixels region and the nearby breast region will be formed. This edge might be falsely detected as the pectoral muscle boundary later on (Rahman and Jha, 2022). Therefore the Zero Background Pixel Correction algorithm by (Rahman and Jha, 2022) was performed on the inpainted ROI, where each row is scanned and if a 0-pixel is detected, the mean intensity value of 12 nearby nonzero pixels along the same row will be assigned to all 0-pixels in that row.

2.1.2 Multidirectional Gabor Filter (MGF)

After the ROI Preprocessing step, a set of three high-frequency Gabor filters tuned at different orientations was created and applied to the processed ROI for capturing the PMB. The parameter values were selected as follows:
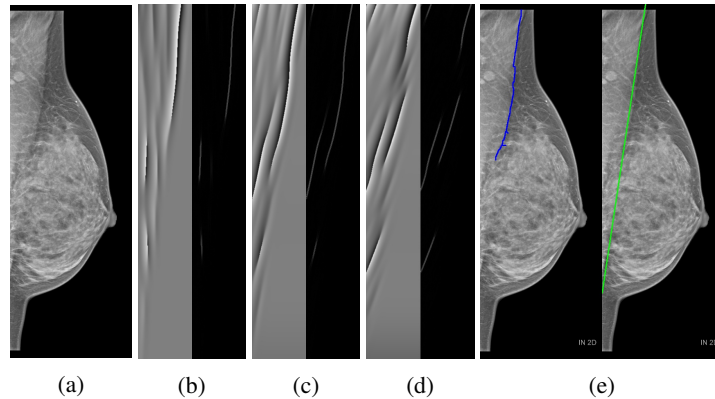
(a)   (b)   (c)   (d)   (e)

Figure 1: (a) Source image. (b, c, d) Phase response (left) and Laplacian (right) for orientations 180, 170 and 160 respectively. (e) Detected pectoral muscle boundary (left) marked in blue and fitted line marked in green (right).

1. The three Gabor filters were each tuned to an orientation (α) of 180, 170 and 160, respectively, to cover all orientations in which the muscle can appear.

2. The spatial aspect ratio was set to the value 0.2617 obtained by using the formula $\frac{3*\pi}{2*M}$ stated in (Rahman and Jha, 2022) with $M = 18$, where M denotes the total number of filters in the interval $[0, \pi]$.

3. The spatial frequency bandwidth was set to 1.2 octaves allowing a moderate range of frequencies around the central frequency in which the filter can respond well.

4. The wavelength (λ) was set in a similar manner as in (Rahman and Jha, 2022) and was computed using the formula $\lfloor \frac{w}{2} * \frac{\sqrt{2}}{4} \rfloor$ where w denotes the width of the ROI image to capture high- and mid-frequency features.

2.1.3 Phase Response of MFG for Pectoral Muscle Detection

After applying the three Gabor filters to the ROI image, the phase response of each Gabor response image was computed. To detect and extract the textural edge information the Laplacian of each phase response was computed and combined (addition) (Rahman and Jha, 2022). The combined Laplacian image (Fig. 1b,c,d) was converted into a binary image by applying simple thresholding with a threshold value of 8. In some cases, a strong intensity edge might be reflected in two or three phase responses, and because of this two or three different intensity edges very close to each other might appear in the combined Laplacian (Rahman and Jha, 2022). Morphological closing (filling small holes) was applied to the resulting image in order to merge nearby edge lines. The PMB was obtained by selecting the largest connecting compo-

nent with 8-connectivity. Once the pectoral muscle had successfully been detected, a line was fitted to the points on the detected boundary using the linear least squares method. This is necessary because the actual PMB is curved, but for computing the PNL length a straight line is needed (Fig. 1e).

3 NIPPLE DETECTION

3.1 ROI Extraction

For detecting the nipple only a small region is of interest and therefore a small ROI containing the nipple was extracted. This was done similarly as in (Jiang et al., 2019). First, the topmost corner marking the starting point of the breast boundary (x_1, y_1) computed in figure 2.1 and the bottom-left corner (x_2, y_2) were used as ending points for forming a line. The angle θ required for rotating this line so that it aligns with the left image border was calculated

$$line\_angle = \left| tan^{-1}(\frac{y_1 - y_2}{x_1 - x_2}) \right| * \frac{180}{\pi} \quad (1)$$

$$\theta = | line\_angle - 90 |. \quad (2)$$

Then the breast mask computed in figure 2.1 was rotated (only necessary for the MLO view) by θ and passed to the border following algorithm (Suzuki and Keiichi, 1985) to get the breast contour, the rightmost point on the contour was identified and shifted by 35 pixels to the left along the x-axis. A new image with the same shape as the breast mask filled with 0-pixels was then created. Pixel values of pixels lying inside the rectangular region bounded by the corner points $(s_x, 0)$, $(w, 0)$, (w, h) and $(s_x, 0)$ were set to 255 where (s_x, s_y) are the coordinates of the shifted point, w is the width and h is the height of the image. Afterwards,

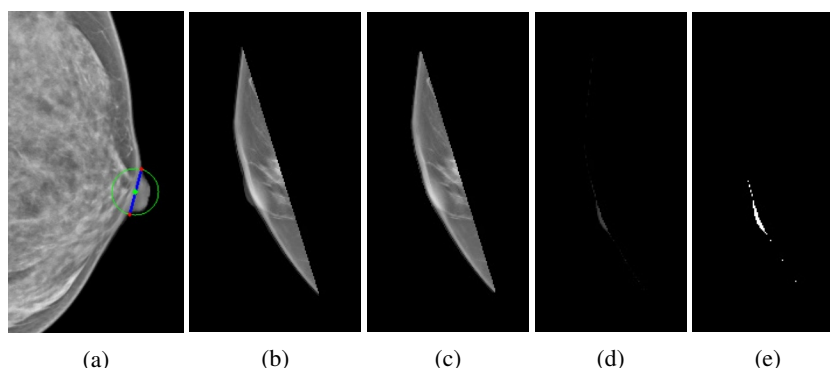(a)   (b)   (c)   (d)   (e)

Figure 2: (a) Starting points are marked with red circles and the location of the nipple base is marked with a green circle. (b) Breast with nipple. (c) Breast without nipple. (d) Output of intersection between (b) and (c). Thresholded image of (d).

bitwise conjunction between the rotated breast mask and the new image was performed. The new mask was then rotated back to its original position (only for the MLO view). To get the ROI containing only the nipple region bitwise conjunction between the mask and the source image was performed.

3.2 Detection of the Nipple

First, large nipples that are in profile are located. Here, the ROI image was converted into a binary image, and the contour of the nipple region was computed following the border (Suzuki and Keiichi, 1985). Then the convex hull of the nipple region was computed which is the minimum boundary that encloses this region. Afterwards, the convexity defects (deviations of the contour from the convex hull), are calculated. Large deviations with a depth greater than 2.5 usually indicate the starting points of the nipple. The two points with the largest deviation (x_1, y_1) and (x_2, y_2) were used to find the location of the nipple base $\left(\frac{x_1+x_2}{2}, \frac{y_1+y_2}{2}\right)$ (Fig. 2a).

If no deviation with a depth greater than 2.5 was found, either a small nipple in profile or a subtle nipple was present, a problem that was overcome as explained next. Usually, small nipples that are in profile have a distinct nipple base boundary edge and this characteristic was used to detect them. This was done by segmenting the nipple from the rest of the breast using watershed segmentation (Meyer, 1992). A marker was created by determining which region belongs to the breast region without the nipple (sure foreground) and which is the background (sure background). To obtain the sure background, dilation (adds pixels to the object boundaries) with a 2×2 kernel consisting of ones was applied to the binary image and for the sure foreground, we applied erosion (removes pixels from boundaries) with a 12×12 kernel. By subtracting the sure foreground from the sure background, a region (unknown) was derived for

which there is no information on whether it belongs to the foreground or background. This unknown region encloses the nipple base boundary edge. Next, the regions in the marker are labelled. The unknown region was labelled with 0, the background with 1 and the foreground with 2. The marker was then passed to the watershed segmentation algorithm to get the contour of the breast region without the nipple. Next, the intersection between the breast region and the breast region without the nipple was computed followed by thresholding. The largest connecting component with an area greater than 25 was selected as the nipple (Fig. 2).

If no connecting component with an area greater than 25 was found, a subtle nipple (nipple not in profile) was present. For detecting subtle nipples the source image was first restricted to the region along the breast boundary. Next, Non-Local Means Denoising was applied to the ROI image to reduce noise, followed by opening (removing small objects from the foreground) with circular structuring element of size 10×10. Afterwards, Hough Circle Transform was applied to find circles with a circle radius between 10 and 25, and only those with a mean intensity greater than 65 were selected. The final subtle nipple is the circle furthest to the right.

3.3 Posterior Nipple Line Computation

Once the pectoral muscle and nipple have successfully been detected, the posterior nipple line and its length can be computed. Here, the pectoral muscle is represented as a tuple (m_{pec}, c_{pec}) where m_{pec} is the slope and c_{pec} is the y-intercept in the slope-intercept form $y = m * x + c$ of the pectoral muscle line. If the muscle line cannot be represented in slope-intercept form, that is, it is a vertical line, the pectoral muscle is represented by the variable x_{pec} instead, which is set to the value of the x-coordinate of any point on that line. The nipple is represented by its coordinates
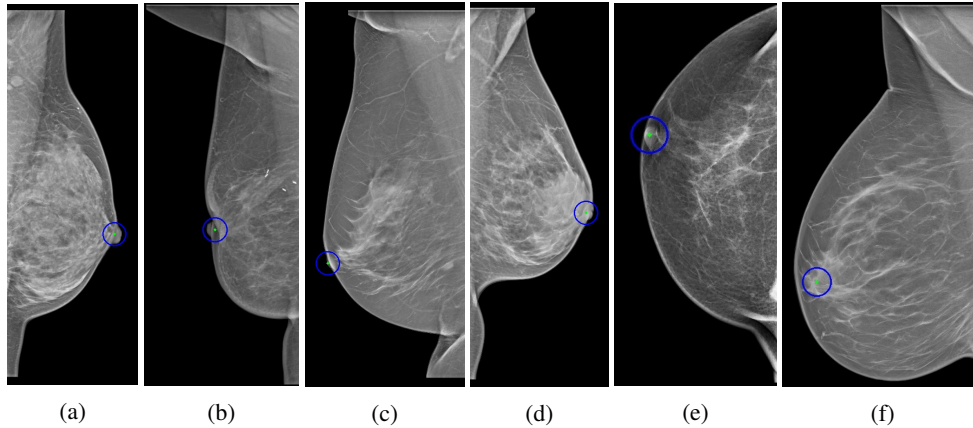
Figure 3: Examples of correctly (a) and falsely (b) located nipples that are in profile and large. Examples of correctly (c) and falsely (d) located nipples that are in profile and small. Examples of correctly (e) and falsely (f) located nipples that are not in profile.

(x_{nip}, y_{nip}).

In the case where the pectoral muscle is not a vertical line, the slope m_{pnl} and the y-intercept c_{pnl} of the linear equation of the PNL were calculated as follows:

$$m_{pnl} = \frac{-1}{m_{pec}} \qquad (3)$$

$$c_{pnl} = (y_{nip} - (m_{pnl} * x_{nip})) \qquad (4)$$

Next, the intersection point (x_{inter}, y_{inter}) of the pectoral muscle line and the PNL line was calculated as follows:

$$\begin{bmatrix} x_{inter} \\ y_{inter} \end{bmatrix} = \begin{bmatrix} -m_{pnl} & 1 \\ -m_{pec} & 1 \end{bmatrix}^{-1} \begin{bmatrix} c_{pnl} \\ c_{pec} \end{bmatrix} \qquad (5)$$

In the case where the pectoral muscle is a vertical line, the PNL is a horizontal line with linear equation $y = y_{nip}$ and the intersection point is (x_{pec}, y_{nip}).

To calculate the length of the PNL, the Euclidean distance between the intersection point and the nipple was calculated.

4 EXPERIMENTAL EVALUATION

A dataset of DICOM images provided by the Medical University of Innsbruck was used in our experimental evaluation, which contains mammograms of both MLO and CC views. For each patient there is an MLO and a CC view of each breast (left and right), for some patients, there are only images of one side of the breast.

4.1 Qualitative Results on Nipple Detection

Nipples that were large and had well-defined edges at the two starting points of the nipple were accurately identified in most of the cases as shown in figure 3a. In cases with no sharp edges, the center could be slightly off since the points with the largest deviation can not be accurately defined. Our approach failed to detect the nipple in rare cases as the one shown in figure 3b, which was due to the breast having an indentation at the location of the nipple.

Our approach was also successful at detecting small nipples that are in profile. This is because the edge of the nipple base is usually well-defined making proper segmentation possible (Fig. 3c). If a small nipple in profile was present but the nipple base edge was not well-defined, our method failed to correctly locate the nipple (Fig. 3d), but this case rarely occurred.

The detection of nipples that are not in profile (subtle nipples) is a challenging task even for experts since in most cases the nipple is not clearly visible or not visible at all. Therefore the performance of the proposed method for detecting nipples for this case was not good. We obtained good results in cases where the nipple had a round shape and well-defined edges (Fig. 3e). For cases where the shape of the nipple was not round or its edges were not well-defined, the Hough Circle Transform failed to accurately identify the nipple. The center could be slightly off. There were also some cases where the nipple was not visible at all (Fig. 3f).

4.2 Qualitative Results on Pectoral Muscle Detection

The proposed method for pectoral muscle detection was very accurate for PMBs that have well-defined edges as in figure 4a. If dense breast tissue is present around the border but the edge is still defined, the border can be still accurately identified (Fig. 4b). The
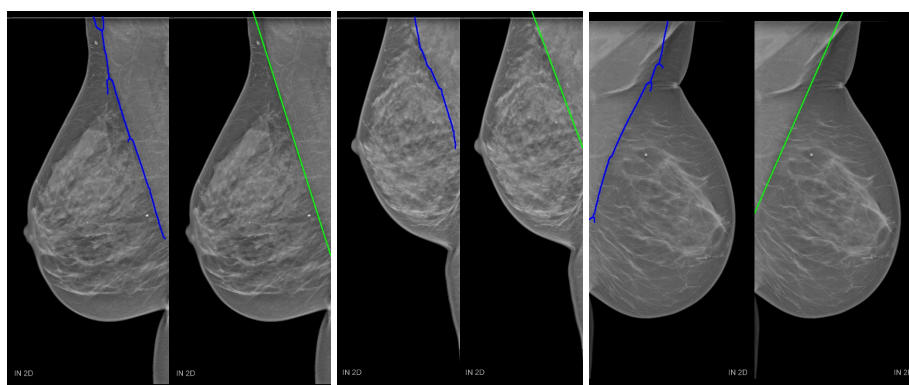
(a)   (b)   (c)

Figure 4: Examples of correctly located PMB. The detected edge is marked in blue and the fitted line to the detected edge is marked in green.

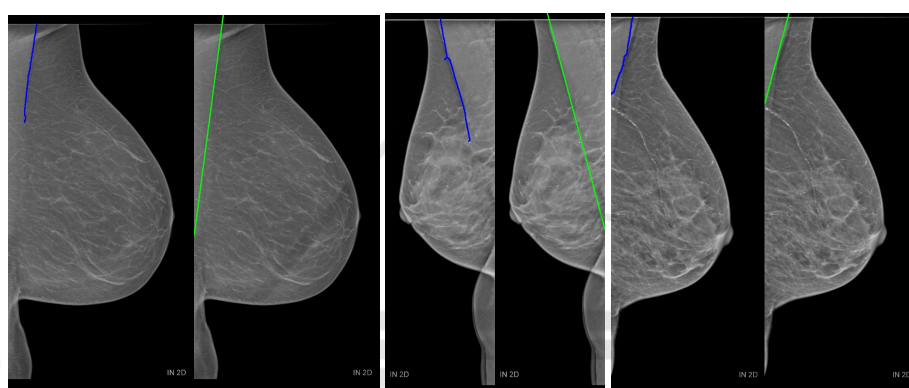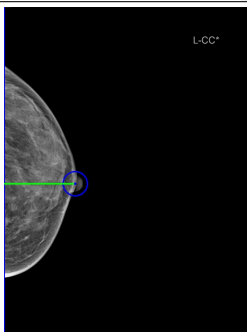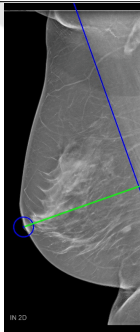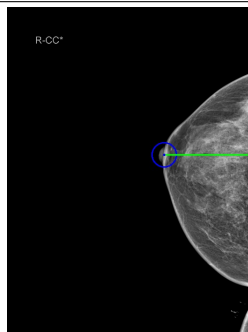(a)   (b)   (c)

Figure 5: Examples of falsely located PMB. The detected edge is marked in blue and the fitted line to the detected edge is marked in green.

Table 1: Examples for computed PNL that were close to the expert values. PNL is marked in green. Values are in mm.
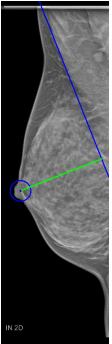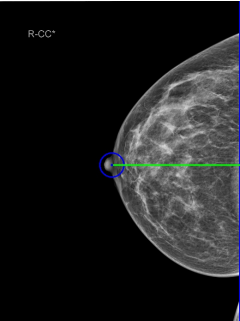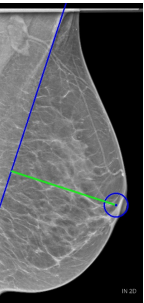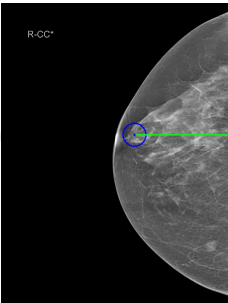

True PNL: 98.90 mm	True PNL: 50.80 mm	True PNL: 114.70 mm	True PNL: 61.40 mm
Computed PNL: 99.72 mm	Computed PNL: 54.11 mm	Computed PNL: 114.30 mm	Computed PNL: 65.15 mm
Difference: 0.82 mm	Difference: 3.31 mm	Difference: 0.40 mm	Difference: 3.75 mm

breast tissue here does not affect our method since it will be removed during the inpainting step. In figure 4c the PMB was accurately located even with a occurring fold close to the border. Since the fold has high-

intensity pixels it was removed during the inpainting step and therefore was not falsely detected as an edge.

There were a few cases where our method failed to correctly locate the PMB. An example is shown

Table 2: Examples for computed PNL that were off when compared to the expert's. PNL is marked in green. Values are in mm.

Examples	Analysis	Examples	Analysis
	True PNL: 92.00 mm Computed PNL: 78.41 mm Difference: 13.59 mm Here the computed PNL length is shorter than the true length. The pectoral muscle is strongly curved and therefore the located boundary is off.		True PNL: 85.90 mm Computed PNL: 98.61 mm Difference: 12.71 mm Here the computed PNL length is longer than the true length. The PNL was measured from the nipple to the right image border but should have been measured from the nipple to the pectoral muscle (not visible).
	True PNL: 88.80 mm Computed PNL: 86.56 mm Difference: 2.24 mm Here there is a small difference because the nipple (in profile and large) was not located accurately and is slightly off.		True PNL: 84.80 mm Computed PNL: 76.54 mm Difference: 8.26 mm Here the nipple (not in profile) was falsely detected, which led to a large difference between the actual and computed PNL length.

in figure 5a, here the upper part of the PMB could be accurately identified since a strong intensity edge is present, whereas the lower part is strongly blurred and could not be captured by the Gabor filters. In this case, using only the upper part to determine the real PMB did not suffice. The second example is similar to the previous one except that the problem lies in the fact that there was dense breast tissue. Therefore the detected border was slightly off (Fig. 5b). Another example of a failure can be seen in figure 5c, where multiple edges that are close to each other are present making it difficult to identify the real PMB. Even if the PMB can be accurately detected, fitting the line to the detected edge can still result in a falsely marked PMB. This is only the case if the actual pectoral muscle is strongly curved.

4.3 PNL Quantitative Results

For evaluating the performance of the proposed method 100 images from the dataset were used. Images with breast implants, not visible nipples, or missing real PNL length (manually measured by an expert from the Medical University of Innsbruck) were not considered. The computed PNL length was compared with the real PNL length. When using those 100 images, we obtained an absolute mean error of just 6.39

mm (stdev.= 4.62 mm). Since the location of both the PMB and the nipple are needed for calculating the PNL length, both of them need to be accurately located, It would be enough for just one component to be incorrectly detected to have a negative impact on the overall performance. In table 1 four examples (two for each view) with their results can be seen. The nipples were accurately located in all of them, and the boundaries of the pectoral muscle were also correctly identified in the MLO views. Table 2 shows four examples of a few cases were results were worse than expected along with an explanation on the causes.

5 CONCLUSIONS

This thesis presents a method to automatically compute the length of the PNL in mammograms, which can be divided into three parts: Pectoral Muscle Detection, Nipple Detection, and PNL Computation. For the detection of the PMB, a set of three phase responses was computed by using three high-frequency Gabor filters tuned at three different orientations. The Laplacian was then computed for each phase response and combined to detect the muscle boundary. For the nipple detection method, the convex hull of the nipple region was used to calculate the convexity de-

fects. Based on this, a distinction could be made between large and small nipples. Large nipples can be located by using the two points with the largest deviation (depth greater than 2.5 each) and small nipples were located with the help of watershed segmentation. If no nipple could be found, it means that the nipple does not lie on the breast boundary and for this case, Hough Circle Transform was used. Once both the PMB and nipple were detected, the PNL length was calculated.

By applying the proposed method on 100 images from the dataset provided by the Medical University of Innsbruck an absolute mean error of 6.39 mm could be achieved. In cases where the nipple does not lie along the breast boundary, the method performs poorly, but otherwise, the accuracy is high, except for some rare cases. The overall performance of the detection of the PMB is very accurate, although there is still room for improvement for some cases.

ETHICS APPROVAL

This study was approved by the ethics commission of the Medical University of Innsbruck (reference number 1321/2021).

REFERENCES

Bertalmio, M., Sapiro, G., Caselles, V., and Ballester, C. (2000). Image inpainting. In *Proceedings of the 27th Annual Conference on Computer Graphics and Interactive Techniques*, SIGGRAPH '00, page 417424, USA.

Brahim, M., Westerkamp, K., Hempel, L., Lehmann, R., Hempel, D., and Philipp, P. (2022). Automated assessment of breast positioning quality in screening mammography. *Cancers*, 14(19).

Buades, A., Coll, B., and Morel, J. (2011). Non-Local Means Denoising. *IPOL*, 1:208–212.

Deng, J., Dong, W., Socher, R., Li, L., Kai, L., and Li, F. (2009). Imagenet: A large-scale hierarchical image database. In *CVPR 2009*, pages 248–255.

Gupta, V., Taylor, C., Bonnet, S., Prevedello, L., Hawley, J., White, R., Flores, M., and Erdal, B. (2020). Deep learning-based automatic detection of poorly positioned mammograms to minimize patient return visits for repeat imaging: A real-world application.

Harris, C. and Stephens, M. (1988). A combined corner and edge detector. In *Proceedings of the Alvey Vision Conference*, pages 23.1–23.6. doi:10.5244/C.2.23.

Hejduk, P., Sexauer, R., Ruppert, C., Borkowski, K., Unkelbach, J., and Schmidt, N. (2023). Automatic and standardized quality assurance of digital mammography and tomosynthesis with deep convolutional neural networks. *Insights into Imaging*, 14(1):90.

Jiang, J., Zhang, Y., Lu, Y., Guo, Y., and Chen, H. (2019). A radiomic-feature based nipple detection algorithm on digital mammography. *Medical Physics*, 46.

Klabunde, C., Bouchard, F., Taplin, S., Scharpantgen, A., and Ballard-Barbash, R. (2001). Quality assurance for screening mammography: an international comparison. *JECH*, 55(3):204–212.

Meyer, F. (1992). Color image segmentation. In *1992 International Conference on Image Processing and its Applications*, pages 303–306.

Pizer, S., Amburn, E., Austin, J., Cromartie, R., Geselowitz, A., Greer, T., ter Haar Romeny, B., Zimmerman, J., and Zuiderveld, K. (1987). Adaptive histogram equalization and its variations. *CVGIP*, 39(3):355–368.

Rahman, M. and Jha, R. (2022). Multidirectional gabor filter-based approach for pectoral muscle boundary detection. *IEEE TRPMS*, 6(4):433–445.

Sung, H., Ferlay, J., Siegel, R., Laversanne, M., Soerjomataram, I., Jemal, A., and Bray, F. (2021). Global cancer statistics 2020: Globocan estimates of incidence and mortality worldwide for 36 cancers in 185 countries. *CA*, 71(3):209–249.

Suzuki, S. and Keiichi, A. (1985). Topological structural analysis of digitized binary images by border following. *CVGIP*, 30(1):32–46.

Sweeney, R., Lewis, S., Hogg, P., and McEntee, M. (2017). A review of mammographic positioning image quality criteria for the craniocaudal projection. *The British journal of radiology*, 91 1082:20170611.

Szegedy, C., Vanhoucke, V., Ioffe, S., Shlens, J., and Wojna, Z. (2015). Rethinking the inception architecture for computer vision.

Waade, G., Skyrud, D., Holen, A., Larsen, M., Hanestad, B., Hopland, N., Kalcheva, V., and Hofvind, S. (2021). Assessment of breast positioning criteria in mammographic screening: Agreement between artificial intelligence software and radiographers. *Journal of Medical Screening*, 28:096914132199871.